Journal of Catalysis **193,** 176–185 (2000)
doi:10.1006/jcat.2000.2893, available online at http://www.idealibrary.com on IDEAL®

XAFS Study of Tin Modification of Supported Palladium Catalyst for 1,3-Butadiene Hydrogenation in the Presence of 1-Butene

Sun Hee Choi and Jae Sung Lee[1]

Department of Chemical Engineering, Pohang University of Science and Technology (POSTECH), San 31 Hyoja-dong, Pohang 790-784, Republic of Korea

Received July 13, 1999; revised April 13, 2000; accepted April 14, 2000

Alumina-supported palladium catalyst, which is active for the hydrogenation of 1,3-butadiene, was modified by tin using various tin precursors. The structure of modified catalysts was studied by XAFS and TPR. Before modification, palladium on alumina existed in an electron-deficient hydride state, which was revealed by a shift to a higher Pd K-edge energy in XANES and by an increased Pd–Pd distance in EXAFS fitting. However, tin modification caused the palladium edge energy to decrease to the value of zero valent palladium metal and destroyed the Pd ensembles by making Pd–Sn bonds, irrespective of the nature of tin precursor. This was responsible for the increased 1-butene selectivity in the hydrogenation of 1,3-butadiene in the presence of 1-butene. A carbonaceous species was formed in the catalyst modified with an organic tin precursor, while the inorganic tin modification produced a tin oxide-like species in addition to the formation of Sn–Pd bonds. © 2000 Academic Press

Key Words: **XAFS; 1,3-butadiene hydrogenation; Pd catalyst; tin modification.**

INTRODUCTION

A number of studies have been devoted to the selective hydrogenation of 1,3-butadiene to butene since the 1960s (1). Modern industrial processes use the selective hydrogenation over supported Pd catalysts for the purification of petrochemical products generated from cracking units by removing acetylene in the ethylene cut and 1,3-butadiene in the butene-rich cut. There have been some recent studies of the selective hydrogenation of 1,3-butadiene in the presence of 1-butene. Riley (2) studied the vapor-phase kinetics of the reaction at low pressures and moderate temperatures. On palladium supported on zinc oxide showing a strong metal–support interaction, it was found that the hydrogenation was not entirely selective, as even in the early stage of the reaction *n*-butane was formed and 1-butene was isomerized to *cis*- and *trans*-2-butene (3). It was suggested that the hydrogenation was inhibited while isomerization of 1-butene still proceeded, which produced the negative selectivity of 1-butene. On the other hand, addition of a second metal improved the selectivity. Addition of cobalt to a palladium catalyst extended the region of positive 1-butene selectivity from 85% to over 90% butadiene conversion for 1 wt% Pd and to over 99% conversion for 0.1 wt% Pd catalysts, and decreased the amount of *n*-butane at comparable conversions (4). Addition of copper to alumina-supported palladium improved the catalytic selectivity for partial hydrogenation of 1,3-butadiene in the presence of a large excess of 1-butene (5).

Catalyst modification with tin has been extensively studied for Pt–Sn re-forming catalysts where an inorganic tin precursor such as stannic chloride or stannous chloride was adopted (6, 7). With the purpose of controlling the properties of the bimetallic catalyst, a new preparation method has been employed, in which organometallic compounds react with pre-formed platinum metal on the support. Thus Margitfavi *et al.* (8, 9) suggested that alkyl tin compounds reacted with hydrogen adsorbed on platinum to yield Pt–Sn bimetallic clusters and alkanes (8, 9). However, in more detailed studies of other supported bimetallic catalysts using solid-state NMR and STEM-EDAX, it was suggested that bimetallic species with organometallic fragments were formed such as $Rh[Sn(n\text{-}C_4H_9)_x]_y$ ($1 < x < 3$, $0 < y < 1$) and $Ni_zSn(n\text{-}C_4H_9)_x$ by the controlled hydrogenolysis of tetrabutyltin (10, 11).

In the present work, we have studied alumina-supported palladium catalysts modified by tin, to improve the 1-butene selectivity in the hydrogenation of 1,3-butadiene in the presence of 1-butene. The palladium catalysts modified with organometallic tin have been studied by X-ray absorption fine structure (XAFS) spectroscopy. The extended X- ray absorption fine structure (EXAFS) reveals information on the local atomic arrangement about each individual type of an absorber atom and the X-ray absorption near-edge structure (XANES) contains information on the electronic structure, the chemical environment, and the oxidation state of the absorber (12). This structural and chemical information is correlated with the catalytic activity for the

[1] To whom correspondence should be addressed. E-mail: jlee@postech.ac.kr. Fax: 82-562-279-5799.

0021-9517/00 $35.00
Copyright © 2000 by Academic Press
All rights of reproduction in any form reserved.

selective hydrogenation of 1,3-butadiene in the presence of 1-butene.

EXPERIMENTAL

Catalyst Preparation

The supported palladium catalysts were prepared by a wet impregnation technique with 2 wt% loading of the metal. After palladium chloride ($PdCl_2$, Aldrich) was dissolved in aqueous ammonium hydroxide, a solution of a metal salt was loaded into pores of γ-Al_2O_3 (Strem Chemicals, BET surface area = 164.1 $m^2\,g^{-1}$). The solvent was then evaporated, and the powders were dried at 353 K for 12 h. Treatment in a hydrogen flow at 423 K for 4 h resulted in reduced Pd/Al_2O_3 catalysts.

A tin modification of the well-reduced palladium catalyst was done following Stytsenko (13). Two kinds of tin precursors were used. Inorganic precursors were tin(II) chloride ($SnCl_2$, Aldrich) and tin(IV) chloride ($SnCl_4$, Aldrich), and organic ones included tetrabutyltin ($Sn(n\text{-}C_4H_9)_4$, Aldrich) and tetraallyltin ($Sn(H_2C{=}CHCH_2)_4$, Aldrich). A measured volume of the solution containing tin compounds (an atomic ratio Sn/Pd = 1) was added to about the same volume of the Pd/Al_2O_3 catalyst under hydrogen atmosphere by a wet impregnation technique. Then, the modified catalysts were prepared by drying at 423 K for 1 day. The solvents used were ethanol for inorganic tin precursors and benzene for organic precursors. As references, monometallic tin catalysts were also prepared by the same wet impregnation method. If not specified otherwise, all catalysts were reduced in H_2 flow at 773 K for 2 h before spectroscopic analysis or catalytic reaction.

XAFS Measurements and Data Analysis

The catalysts were pressed into self-supporting wafers for the XAFS measurements. The sample disc was placed in a controlled atmosphere XAFS cell designed for *in situ* experiments (14). The catalyst wafers in the U-tube reactor attached to the spectroscopic cell were treated in flowing hydrogen at 773 K for 2 h. The sample was transferred to the cell from the reactor and isolated by sealing off the glass connection, with the sample still under the same gas atmosphere as that used for the treatment.

XAFS measurements for the samples in the sealed spectroscopic cell were performed on BL10B of Photon Factory (KEK) in Japan (15, 16). All spectra were taken at room temperature in a transmission mode for K-edges of Pd and Sn. In particular, the integration time for data acquisition was 3 s per data point in Pd spectra and 6 s per data point for Sn spectra because of low photon fluxes at high absorption edge energies. Electron currents used during X-ray absorption measurements were between 250–400 mA and the intensities for incident and transmitted beams were measured by two ionization chambers. Detector gases for the incident beam were argon for both K-edges of Pd and Sn, and those for the transmitted beam were argon for Pd K-edge and krypton for Sn K-edge.

The obtained XAFS data were analyzed with the UWXAFS 3.0 package (17) and the FEFF 7 code (18), both of which had been licensed from the University of Washington. The pre-edge background was removed by using a linear fit and post-edge background function was obtained with a spline that could be adjusted so that the low R component of pre-Fourier transformed data $\tilde{\chi}(R)$ were minimized. The EXAFS function, then, could be obtained from $\chi(E) = [\mu(E) - \mu_0(E)]/\Delta\mu_0(E_0)$ where $\mu(E)$ is the absorption coefficient due to the particular edge of the element of interest, $\mu_0(E)$ is the atomic-like absorption, and $\Delta\mu_0(E_0)$ is the jump at the edge step. After that, the power-scaled EXAFS function $k^n\chi(k)$ in momentum space was converted to real space by the Fourier transformation to produce the radial structural function (RSF). A Hanning window sill was used to reduce the truncation effect from Fourier transformation over a finite range. The EXAFS fittings were performed in R-space without Fourier filtering where theoretical standards were synthesized with the FEFF code.

CO Chemisorption and Temperature-Programmed Reaction

The CO chemisorption was performed with a conventional volumetric adsorption apparatus (Micrometrics Model ASAP 2010C). About 0.5 g of catalyst was loaded into a cell for chemisorption, reduced in flowing H_2, and then purged with He at room temperature to remove all hydrogen adsorbed during the reduction. Before measurement of CO uptake, the sample was evacuated at room temperature to a pressure less than 10^{-3} Pa. The first CO adsorption isotherm was taken at increasing CO pressures. Following evacuation at room temperature, the second isotherm was taken in a similar way. The amount of irreversible CO uptake was obtained from the difference between the two isotherms, extrapolated to zero pressure.

For the palladium catalyst modified with tetrabutyltin, temperature-programmed reaction (TPR) was carried out to investigate the interaction between the palladium surface and tetrabutyltin. Pure hydrogen was passed at a flow rate of 20.5 μmol/s through a catalyst bed containing 10 mg of sample. The gas products were analyzed with an on-line mass-selective detector system (HP 5972). The temperature was increased from room temperature to 1173 K at a ramping rate of 10 K/min.

1,3-Butadiene Hydrogenation

The performance of catalysts was tested for the hydrogenation of 1,3-butadiene both in the absence and in the presence of 1-butene. Using a continuous isothermal

reactor at atmospheric pressure, the catalyst was reduced in a hydrogen flow for 2 h at 773 K before the reaction. The reaction was performed at 373 K with a 1,3-butadiene/1-butene/H_2/He mixture 0.23/0/0.34/99.43 (vol%) or 0.15/1.52/0.23/98.10 in the absence and in the presence of 1-butene. The effluent stream from the reactor was analyzed by an on-line gas chromatograph (HP 5890 Series II) equipped with a flame ionization detector (FID) and a 20% BMEA packed column (7.3 m long, 3.2 mm diameter) at 308 K. Product selectivities were calculated as number of the moles of that product formed divided by the number of moles of butadiene consumed (3). The reaction rate was expressed as the number of moles of 1,3-butadiene consumed per second per mole of total palladium.

RESULTS

Hydrogenation of 1,3-Butadiene

The CO uptakes for all catalysts are given in Table 1. Even before the addition of tin, Pd/Al_2O_3 chemisorbed a relatively low amount of CO, probably due to sintering of Pd during reduction at a high temperature of 773 K. This uptake corresponds to 5.2% of total Pd exposed to the surface. The addition of tin decreased the CO uptake further. In particular, modification by organic tin precursors made CO uptake decrease to less than a fifth of that before tin modification, while catalysts modified by inorganic tin precursor showed smaller reductions in CO uptakes.

The results on the hydrogenation of 1,3-butadiene in the absence of 1-butene are given in Fig. 1. The palladium catalysts modified by tetrabutyltin and tin(II) chloride showed similar rates of 1,3-butadiene conversion, but about 20% higher selectivity for butenes compared to the unmodified palladium catalyst. The difference between the two modifications was not great. Both modified catalysts maintained a good stability, showing no sign of deactivation for ca. 8 h on stream once steady states were attained.

In the presence of 1-butene in the feed, the rate of the reaction decreased a little with time on stream for all catalysts as shown in Fig. 2A. The rate of deactivation followed a sequence of unmodified palladium < modified by tetrabutyltin < modified by tin(II) chloride. In Fig. 2B, the negative selectivity for 1-butene means that 1-butene in the feed stream has been converted to 2-butenes and/or *n*-butane, resulting in net loss of 1-butene during the reaction. Thus, modified catalysts showed a smaller 1-butene loss than the unmodified palladium catalyst. *n*-Butane, an undesired product, was produced by excessive hydrogenation, but its extent was significantly lowered for the catalyst modified by tetrabutyltin, compared to the unmodified catalyst and

TABLE 1

CO Uptakes of Pd–Sn/Al_2O_3 Catalysts at Room Temperature

Sample	CO uptake (μmol/g cat.)
Pd/Al_2O_3	8.99
$Pd–Sn(C_4H_9)_4/Al_2O_3$	1.73
$Pd–Sn(allyl)_4/Al_2O_3$	1.60
$Pd–SnCl_2/Al_2O_3$	5.20
$Pd–SnCl_4/Al_2O_3$	2.32

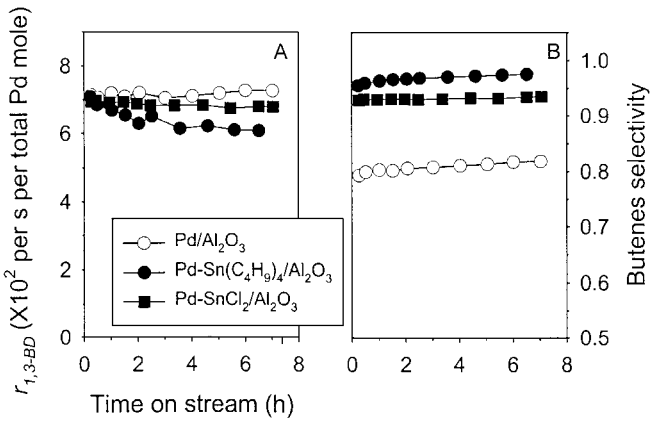

FIG. 1. Hydrogenation of 1,3-butadiene in the absence of 1-butene. (A) Rate of 1,3-butadiene consumption (moles per second per mole of total Pd). (B) Butenes selectivity. Conditions: H_2/1,3-butadiene = 1.5, space velocity = 200,000 l h^{-1} kg^{-1}, T = 373 K.

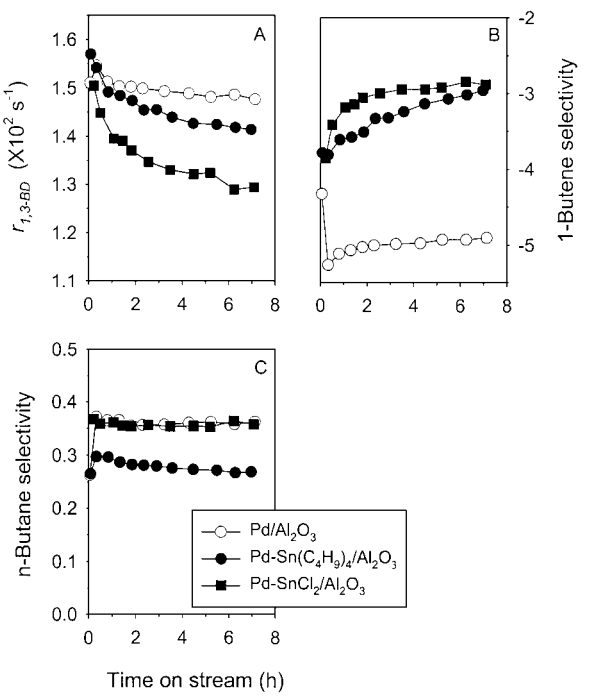

FIG. 2. Hydrogenation of 1,3-butadiene in the presence of 1-butene. (A) Rate of 1,3-butadiene consumption (moles per second per mole of total Pd). (B) 1-Butene selectivity. (C) *n*-Butane selectivity. Conditions: H_2/1,3-butadiene = 1.5, space velocity = 180,000 l h^{-1} kg^{-1}, T = 373 K.

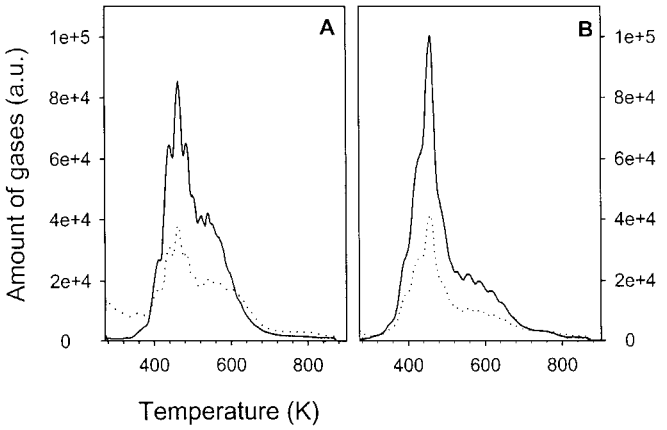

FIG. 3. Temperature-programmed reaction spectra of alumina-supported tin and tin-modified palladium catalysts. (A) $Sn(C_4H_9)_4/Al_2O_3$ and (B) $Pd–Sn(C_4H_9)_4/Al_2O_3$. The solid line is for *n*-butane and the dotted line is for butenes.

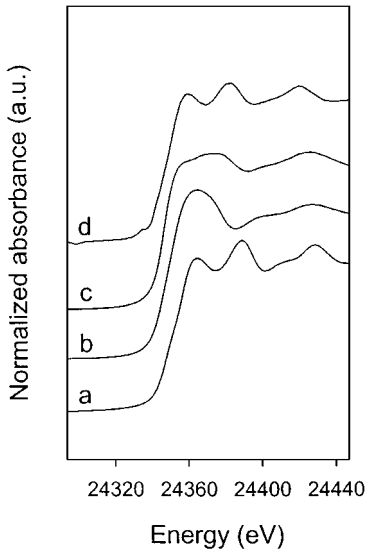

FIG. 4. Pd K-edge XANES of palladium references and alumina-supported palladium catalyst: (a) Pd foil, (b) Pd(II) acetate, (c) $PdCl_2$, and (d) Pd/Al_2O_3.

the catalyst modified by tin(II) chloride. The catalyst modified by tin(IV) chloride exhibited a rate of 1,3-butadiene consumption, and selectivities for 1-butene and *n*-butane similar to those for the catalyst modified by tin(II) chloride. Finally, modification by another organic tin precursor (allyltin) showed nearly the same rate of 1,3-butadiene consumption but a decreased 1-butene selectivity by about 30% and an increased *n*-butane selectivity by 5%, compared to the results of tetrabutyltin-modified catalyst.

Temperature-Programmed Reaction (TPR)

When the tetrabutyltin-modified palladium catalyst was heated in an H_2 flow at increasing temperatures, C_4 hydrocarbons were produced by hydrogenolysis of added organic tin species as shown in Fig. 3. The results of TPR for $Sn(C_4H_9)_4/Al_2O_3$ are also included for comparison. Not only *n*-butane but also butenes were formed for both alumina-supported tin samples and tetrabutyltin-modified palladium catalyst. The maximum peak temperatures were near 450 K for all catalysts. The peak of alumina-supported tin catalyst was broader than that of tetrabutyltin-modified palladium catalysts, indicating the difference in reactivity of tetrabutyltin toward the alumina surface and the palladium surface. Several peaks were superimposed over about a 200 K temperature range, reflecting non-homogeneous reactivity of the hydrogenolysis of butyl groups in both samples.

XANES of Pd K-Edge and Sn K-Edge

The XANES represents an electronic transition from inner electronic level to outer unoccupied levels and contains information on chemical environment and bonding surrounding the X-ray absorbing atom. Figure 4 shows Pd K-edge XANES spectra for palladium references and unmodified palladium catalysts. The absorption edge maximum in each spectrum corresponds to the allowed $1s \rightarrow 5p$ transition, merging into the continuum at higher energies. Pd foil had a distinctly different shape in XANES compared to those of Pd(II) acetate and $PdCl_2$. Palladium supported on alumina showed a spectrum similar to that of Pd foil, indicating that palladium was well reduced prior to the addition of tin. For the modified palladium catalysts, the Pd K-edge XANES spectra are shown in Fig. 5. Regardless of the nature of the tin precursor, the spectra were all similar

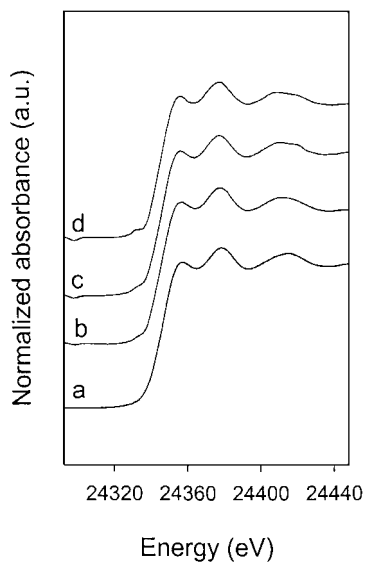

FIG. 5. Pd K-edge XANES of tin-modified palladium catalysts: (a) $Pd–Sn(C_4H_9)_4/Al_2O_3$, (b) $Pd–Sn(allyl)_4/Al_2O_3$, (c) $Pd–SnCl_2/Al_2O_3$, and (d) $Pd–SnCl_4/Al_2O_3$.

TABLE 2

Edge Energy of Palladium References and Catalysts for Pd K-Edge

Sample	Edge energy[a] (eV)
Pd foil	24344.0
Pd(II) acetate	24350.7
$PdCl_2$	24347.4
Pd/Al_2O_3	24346.0
$Pd–Sn(C_4H_9)_4/Al_2O_3$	24344.1
$Pd–Sn(allyl)_4/Al_2O_3$	24344.6
$Pd–SnCl_2/Al_2O_3$	24344.0
$Pd–SnCl_4/Al_2O_3$	24344.3

[a] All were calculated within ±0.4 eV precision.

to that of palladium foil. This indicates that palladium exists in the metallic state in all catalysts.

The edge position in XANES can reveal the oxidation state of the absorbing atom, because it is directly related to the binding energy of the ejected photoelectron during the absorption process. The edge energies for Pd K-edges are given in Table 2. Here, the edge position was calculated as the energy giving the maximal slope in the rapidly rising portion of the absorbance vs energy plot. Compared to the edge energy of Pd foil, the alumina-supported palladium had higher energies by 2.0–2.6 eV. But the energies were still lower than those of Pd(II) compounds. When tin was introduced into palladium, however, the edge energies were decreased to the level of Pd foil. This decrease was observed irrespective of the nature of tin precursor used for the modification.

Sn K-edge XANES spectra are shown for tin references in Fig. 6 and for supported samples in Fig. 7. Although tetrabutyltin does not have ionicity, the shape of XANES was different from that of Sn foil, reflecting a contribution of hydrocarbon backscatters. Thus, the difference between tin metal and tetrabutyltin XANES reflects the difference between metallic bonding and the T_d site symmetry of the SnR_4. Tin oxides gave stronger resonance peaks compared with the edge of Sn foil, which is a general characteristic of oxide species. Alumina-supported tin catalysts (Figs. 7a, 7b) showed resonance shapes similar to those of the tin(IV) oxide. Despite the reduction at the high temperature of 773 K, tin was not reduced on alumina. However, for tin-modified palladium catalysts, the first resonance peak of the tin absorption edge was smaller than those of oxides, and the second and third resonances were barely seen. These were absent in supported tin. These similarities among supported Sn and Sn oxide XANES indicate that tin was not completely reduced to a metallic state and might exist in a mixed oxidation state in catalysts. No particular differences were seen among XANES spectra of $Pd–Sn/Al_2O_3$ catalysts derived from different tin precursors.

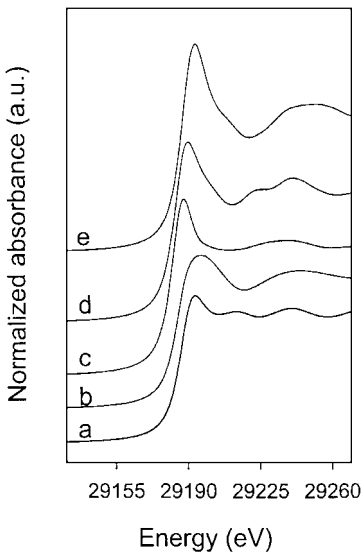

FIG. 6. Sn K-edge XANES of tin references: (a) Sn foil, (b) $Sn(C_4H_9)_4$, (c) $SnCl_2 \cdot 2H_2O$, (d) SnO, and (e) SnO_2.

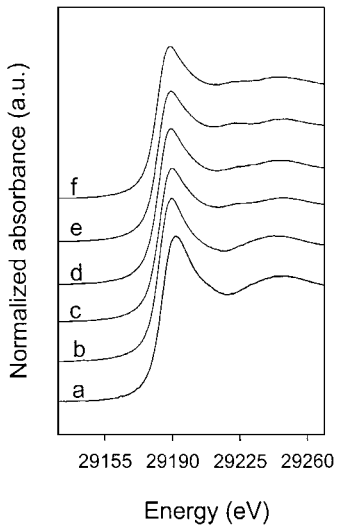

FIG. 7. Sn K-edge XANES of alumina-supported tin and tin-modified palladium catalysts after reduction at 773 K for 2 h: (a) $Sn(C_4H_9)_4/Al_2O_3$, (b) $SnCl_2/Al_2O_3$, (c) $Pd–Sn(C_4H_9)_4/Al_2O_3$, (d) $Pd–Sn(allyl)_4/Al_2O_3$, (e) $Pd–SnCl_2/Al_2O_3$, and (f) $Pd–SnCl_4/Al_2O_3$.

EXAFS of Alumina-Supported Palladium and Tin

The small oscillations in absorbance from 100–1000 eV above the absorption edge were isolated to produce the EXAFS function $\chi(k)$, and ultimately the RSF, as shown in Fig. 8. A peak position in the RSF corresponds to an interatomic distance between absorbing and surrounding scatter atoms displaced from the true distance by a phase shift. The peak intensity is correlated with the average coordination number for the atoms at the distance. The alumina-supported palladium showed palladium metal-like characteristics in both $\chi(k)$ and the RSF. In particular,

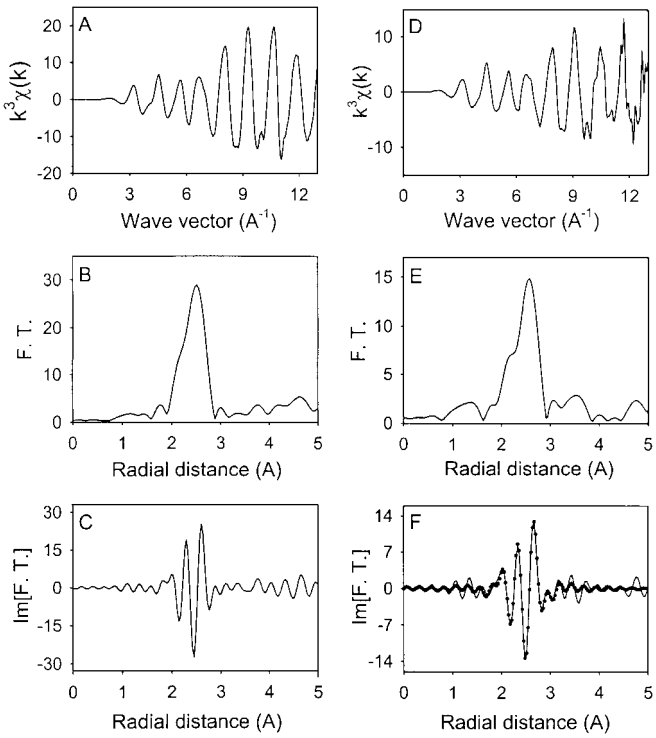

FIG. 8. k^3-weighted EXAFS function (A,D), its Fourier transform (B,E), and the imaginary part of the Fourier transform (C,F) of Pd foil (A–C) and Pd/Al_2O_3 catalyst reduced at 773 K (D–F). The best fit is plotted as the small circles in (F).

the examination of the imaginary part of the Fourier transform shown in Fig. 8C and Fig. 8F is useful, since, due to the phase information, its shape is more characteristic of the types of atoms that make up a given shell.

The magnitude of the Fourier transform from Pd/Al_2O_3 (Fig. 8E) is lower compared with that of palladium foil (Fig. 8B), suggesting that palladium is finely dispersed on Al_2O_3. The fitting results of EXAFS given in Table 3 show it quantitatively. The standard for fitting was the Pd–Pd single scattering which was synthesized with the FEFF code with the known structural information on Pd metal (19). A single adjustable parameter in EXAFS analysis, the amplitude reduction factor (S_o^2) for Pd, was taken to be 0.88, which was found by fitting the experimental RSF of the metal with the theoretical one. The Pd–Pd coordination number was decreased to 8.5 from the bulk value of 12. The Pd–Pd distance in Pd/Al_2O_3 was larger by about 0.05 Å, compared with that of Pd foil.

For alumina-supported tin, the peak at 1–2 Å in the RSF (Fig. 9E) was similar to that of SnO_2 (Fig. 9B). Comparing the imaginary parts of the Fourier transform allowed a clearer identification of the Sn–O peak at 1–2 Å. As a matter of fact, XANES results in Fig. 7 had already suggested that tin in alumina existed in an oxide form. With known structural data on SnO_2 (20, 21), the Sn–O single scattering was used for fitting of Sn/Al_2O_3 catalysts. The amplitude reduction factor for Sn EXAFS fitting was taken to be 0.89. The fitting results are also shown in Table 3.

TABLE 3

EXAFS Curve-Fitting Results of Alumina-Supported Palladium and Tin Catalysts

Sample	N	R (Å)	σ^2 (Å^2)[c]	ℜ-Factor[d]
Pd foil	12.0[a]	2.751		
Pd/Al_2O_3	8.5[a]	2.795	0.0073	0.0060
SnO_2	4.0[b]	2.042		
Sn(C_4H_9)$_4$/Al_2O_3	4.8[b]	2.075	0.0067	0.0050
$SnCl_2$/Al_2O_3	4.8[b]	2.097	0.0116	0.0323

[a] Pd–Pd coordination number.
[b] Sn–O coordination number.
[c] σ^2 = Debye–Waller factor.
[d] ℜ-factor gives a sum-of-squares measure of the fractional misfit, which is defined as $\sum_{i=1}^{N}\{[Re(f_i)]^2+[Im(f_i)]^2\}/\sum_{i=1}^{N}\{[Re(\tilde{\chi}_{\text{data}_i})]^2+[Im(\tilde{\chi}_{\text{data}_i})]^2\}$.

EXAFS of Tin-Modified Palladium Catalyst

For the palladium modified by tetrabutyltin, the EXAFS function and its Fourier transform are shown in Fig. 10. The major peak in the RSF for the Pd K-edge stands at

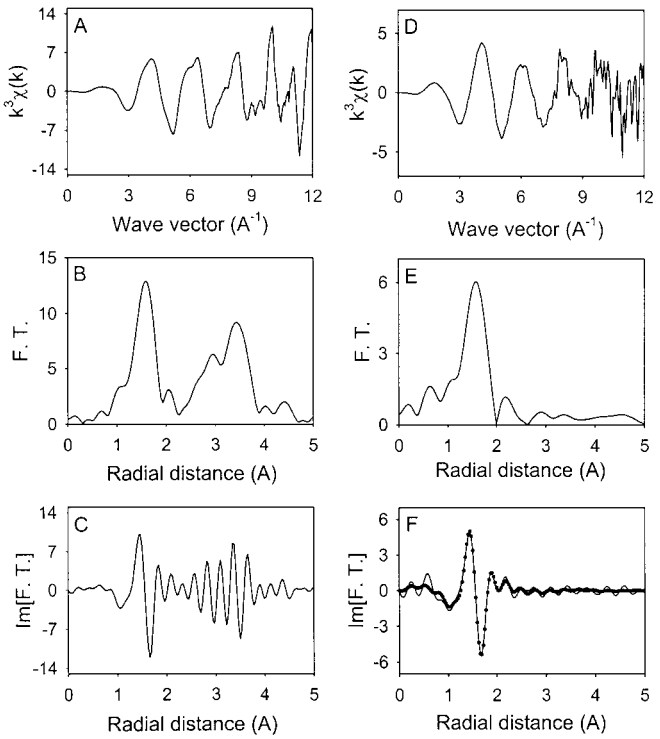

FIG. 9. k^3-weighted EXAFS function (A,D), its Fourier transform (B,E), and the imaginary part of the Fourier transform (C,F) of SnO_2 (A–C) and Sn(C_4H_9)$_4$/Al_2O_3 catalyst reduced at 773 K (D–F). The best fit is plotted as the small circles in (F).

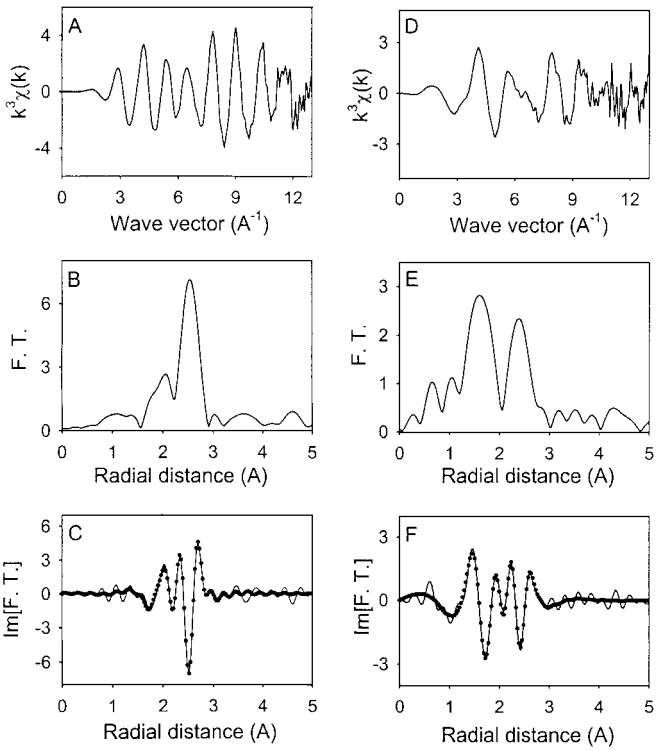

FIG. 10. k^3-weighted EXAFS function (A,D), its Fourier transform (B,E), and the imaginary part of the Fourier transform (C,F) of Pd K-edge (A–C) and Sn K-edge (D–F) of Pd–Sn$(C_4H_9)_4/Al_2O_3$ catalyst. The best fit is plotted as the small circles in (C) and (F).

2–3 Å as in the RSF of the Pd foil. Compared with the EXAFS function of Pd foil (Fig. 8A), however, the modified palladium has some different oscillations in the low wave vector region. This difference appeared as a shoulder to the major peak in RSF of modified palladium. This suggests that the peaks at 1.5–3 Å in RSF are combined contributions of backscatterer Sn as well as backscatterer Pd.

For the Sn K-edge EXAFS, two strong peaks appeared in the RSF, one at 1–2 Å and the other at 2–3 Å. The peak at 1–2 Å is believed to be carbon which remained after hydrogenolysis of $Sn(C_4H_9)_4$ on alumina-supported palladium. This is confirmed by TPR results shown in Fig. 3 and by Fig. 11, in which the peak at 1–2 Å decreases in intensity as the reduction temperature increases. Thus, butyl ligands attached to tin were removed as *n*-butane and butenes as the hydrogenolysis proceeded. As the reduction temperature increased, the decrease in intensity of the peak at 1–2 Å was large, but the intensity of the peak at 2–3 Å increased only slightly up to 473 K and remained constant at higher temperatures. This is well correlated with the result of TPR shown in Fig. 3 where the maximum peak temperature of hydrocarbon evolution is about 460 K. Thus, this peak at 2–3 Å is due to Sn–Pd coordination.

For the nonlinear fitting in *R*-space, two standards for Sn K-edge EXAFS of palladium catalysts modified by tetra-

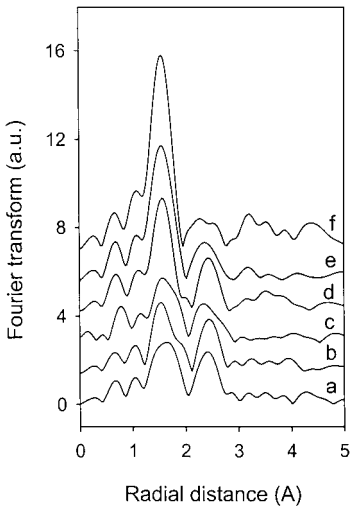

FIG. 11. Fourier transforms of Sn K-edge EXAFS data for Pd–Sn$(C_4H_9)_4/Al_2O_3$ reduced at different temperatures: (a) 773 K, (b) 673 K, (c) 573 K, (d) 473 K, (e) 423 K, and (f) no reduction.

butyltin were used, i.e., Sn–C single scattering for the peak at 1–2 Å and Sn–Pd single scattering for the one at 2–3 Å. However, different standards were adopted for the palladium modified by inorganic tin such as tin(II) chloride or tin(IV) chloride. As shown in Fig. 12, two peaks in RSF are positioned at 1–2 and 2–3 Å for all catalysts. If imaginary parts are compared altogether, the peaks at 2–3 Å have a symmetric shape similar for all catalysts, but peaks at 1–2 Å are distinctly different for inorganic tin modification and organic tin modification. For the catalyst modified with inorganic tin ($SnCl_2$ and $SnCl_4$), the shape of the peaks appeared symmetric, while the catalyst modified with organic tin ($Sn(C_4H_9)_4$ and $Sn(allyl)_4$) showed asymmetric shapes. Therefore, it could be reasoned that the peak at

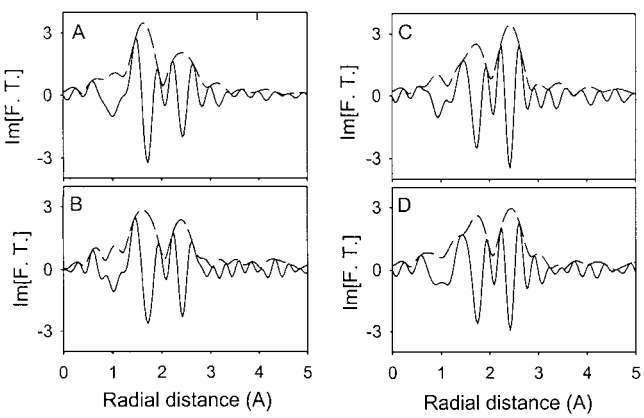

FIG. 12. Fourier transforms of Sn K-edge EXAFS data for the palladium catalysts modified with different precursors: (A) Pd–Sn$(C_4H_9)_4/Al_2O_3$, (B) Pd–Sn$(allyl)_4/Al_2O_3$, (C) Pd–$SnCl_2/Al_2O_3$, and (D) Pd–$SnCl_4/Al_2O_3$. The solid line denotes the imaginary part and the dashed line the magnitude of Fourier transform.

TABLE 4

EXAFS Curve-Fitting Results of Alumina-Supported Palladium Catalysts Modified with Different Tin Precursors

	Shell	N	R (Å)	σ^2 (Å^2)	ℜ-Factor
		A. Sn K-Edge			
Pd–Sn(C_4H_9)$_4$	C	6.2	2.153	0.0112	0.0111
	Pd	5.0	2.638	0.0159	
Pd–Sn(allyl)$_4$	C	5.9	2.166	0.0094	0.0198
	Pd	4.2	2.634	0.0145	
Pd–$SnCl_2$	O	3.2	2.145	0.0157	0.0262
	Pd	3.8	2.650	0.0105	
Pd–$SnCl_4$	O	3.5	2.152	0.0166	0.0278
	Pd	2.0	2.661	0.0071	
		B. Pd K-Edge			
Pd–Sn(C_4H_9)$_4$	Sn	2.4	2.638	0.0110	0.0078
	Pd	6.5	2.793	0.0094	
Pd–Sn(allyl)$_4$	Sn	6.8	2.634	0.0209	0.0396
	Pd	4.0	2.812	0.0089	
Pd–$SnCl_2$	Sn	2.9	2.650	0.0086	0.0429
	Pd	5.5	2.811	0.0130	
Pd–$SnCl_4$	Sn	4.3	2.661	0.0083	0.0174
	Pd	6.6	2.836	0.0127	

1–2 Å for the inorganic tin modification originated from the chlorine or oxygen backscatterer. It is known that the distance of Sn–Cl is 2.66–3.86 Å for tin(II) chloride (22) while tin(IV) chloride has an average distance of 2.280 Å (23). Even though the phase shift is not corrected in the Fourier transform, the peak at 1–2 Å cannot be the contribution of chlorine. Hence, this is due to oxygen, which probably originated from the support Al_2O_3. Furthermore, the effect of the oxygen backscatterer was confirmed by the EXAFS fitting by using Sn–O and Sn–Pd single scattering standards.

After the fitting of Sn K-edge data was performed, the fitting for Pd K-edge was done with the criterion that the distance of Sn–Pd must be equal to that of Pd–Sn. Two standards, Pd–Pd and Pd–Sn single scattering shells, were used for Pd K-edge EXAFS fittings. The fitting results are shown in Table 4.

DISCUSSION

Palladium supported on alumina had a higher Pd K-edge energy compared with palladium foil in XANES. Considering that the shape of resonances is nearly the same as that of palladium foil, it could be concluded that palladium in Pd/Al_2O_3 is in a metallic state. Therefore, the shift to a higher energy reveals that the palladium is in an electron-deficient state. It was also found in EXAFS curve fittings that the Pd–Pd distance increased in Pd/Al_2O_3. These all suggest that the β-hydride phase of palladium was formed in Pd/Al_2O_3 catalyst.

Hydrogen is absorbed into bulk palladium and occupies octahedral interstices of the Pd lattice, even at room temperature under atmospheric pressure of H_2. The lattice structure of palladium hydride represents an isotropically expanded form of the fcc host lattice with the hydrogen atom occupying a part of octahedral sites. It is reported in the literature that at room temperature the best value of lattice constant for pure Pd and for the α- and β-phases of palladium hydrides are 3.890, 3.894, and 4.025 Å, respectively (24). The atomic distance of Pd in our Pd/Al_2O_3 was estimated by EXAFS to be 2.795 Å (Table 3) which gives a lattice constant of 3.953 Å. Thus, a part of Pd in the sample appears to have been transformed to β-hydride. The formation of palladium hydride may also be responsible for the greatly reduced coordination number of 8.5 for Pd/Al_2O_3 although metal dispersion measured by CO chemisorption was only 5.2%. The formation of a nonstoichiometric palladium hydride would enhance the static disorder of Pd–Pd bonds and decrease its apparent coordination number. Increased Pd–Pd distance due to the formation of palladium β-hydride phase agrees well with the result of Davis *et al.* (25). They observed a 3.7% increase in the Pd–Pd distance for Pd–H/Al_2O_3, compared to that for Pd/Al_2O_3. And, in XANES, the edge in the spectrum for Pd–H/Al_2O_3 was higher by 3–4 eV than the edge for the latter.

The XANES clearly shows that the addition of tin to alumina-supported palladium decreased the Pd K-edge energy to the level of palladium foil while maintaining the similar resonance shape, regardless of the nature of tin precursor. This implies that palladium atoms in Pd–Sn/Al_2O_3 catalysts would be under an electronic environment similar to that in Pd metal.

Unlike the Pd K-edge XANES, the edge energy for the Sn K-edge did not reveal any effect of treatment. The obtained edges (in eV) are 29186.8, 29185.3, 29183.4, 29184.7, and 29188.5 for Sn foil, Sn(C_4H_9)$_4$, $SnCl_2 \cdot 2H_2O$, SnO, and SnO_2, respectively. There could not be seen any particular relationship between the edge energy position and the oxidation state of tin. Nevertheless, the shape of resonance in the Sn K-edge is informative. Treatment in a hydrogen flow at a high temperature of 773 K could not convert tin on alumina to metallic tin, which was also confirmed in the EXAFS curve fitting. This result is in complete agreement with that of Nédez *et al.* (26) who observed $>$AlOSn(n-C_4H_9)$_3$ or tetracoordinated tin on the surface of partially dehydroxylated alumina upon addition of hydridotris(butyl)tin onto alumina.

For the palladium catalyst modified by tetrabutyltin, the presence of carbon backscatterer observed in EXAFS was also confirmed by TPR results. The total amount of n-butane plus butenes produced during the hydrogenolysis of tetrabutyltin on alumina-supported palladium was less by 9.0% than that on bare alumina. Because two catalysts were prepared with the same amount of tin, there must exist some

remaining carbon species originating from butyl ligands in palladium catalysts modified by tetrabutyltin. As a matter of fact, some surface organometallic compounds were reported to be formed such as $Rh[Sn(n\text{-}C_4H_9)_x]_y$, $(Ni_s)_zSn(n\text{-}C_4H_9)_x$, and $Pt_s[Sn(n\text{-}C_4H_9)_x]_y$ during the hydrogenolysis of group VIII metals modified with $Sn(n\text{-}C_4H_9)_4$ (10, 11, 27).

In EXAFS curve fitting, the effect of the light backscatterer carbon was remarkable, with Sn–C coordination numbers of 5.9 and 6.2. Together with coordination numbers for Sn–Pd, tin has the large total coordination numbers of 10.1 and 11.2. The large values of Sn–C and Sn–Pd coordination numbers without Sn–Sn interaction suggest that highly dispersed tin may reside in a high coordination surface site of Pd and be covered by a carbonaceous species without forming an organometallic species. In contrast, the effect of the light backscatterer oxygen was clearly represented by reasonable Sn–O coordination numbers of 3.2 and 3.5 for the palladium catalyst modified by inorganic tin compounds.

The Sn–Pd distances are shorter for the palladium modified by organic tin than by inorganic tin, and the coordination number of Sn–Pd is larger for the former. The difference in Sn–Pd coordination numbers obtained from EXAFS fittings is consistent with the results of CO chemisorption. Compared to inorganic tin, organic tin modification causes a much more drastic decrease in CO uptakes of palladium catalyst. Because tin has no affinity to carbon monoxide, the decrease should be correlated to the increased formation of Sn–Pd bonds. Thus, the organic tin compounds interact to a great extent with palladium due to a higher reactivity toward a reduced palladium. According to a theory proposed by Stytsenko (13) small coordination numbers of Sn–Pd for the palladium catalyst modified by inorganic tin could be attributed to higher diffusivity of tin than its reactivity on alumina-supported palladium surface, and thus tin is more likely to migrate away from palladium particles than to react with them. One interesting result is that the Sn–Sn interaction does not appear in EXAFS for any tin-modified palladium catalysts. This indicates that tin remained dispersed in catalysts without self-aggregation. Therefore, it can be suggested that added tin interacts with the palladium surface selectively for catalysts modified by organic tin. On the other hand, a significant fraction of added tin interacts with alumina, showing Sn–O interactions for catalysts modified by inorganic tin.

In the hydrogenation of 1,3-butadiene in the presence of 1-butene, the unmodified palladium catalyst showed the highest 1,3-butadiene consumption rate but a large net loss of 1-butene. In contrast, the modified catalyst exhibited a smaller 1,3-butadiene consumption rate, but also a decreased loss of 1-butene. Among modified catalysts, the organic tin modification made a smaller decrease in 1,3-butadiene consumption rate from the rate for the unmodified Pd catalyst, a comparable 1-butene selectivity, and a decreased *n*-butane selectivity, compared to the modification by inorganic tin. As far as *n*-butane is concerned, the catalyst modified by organic tin produced the least amount of it and the unmodified catalyst and the catalyst modified by inorganic tin produced similar amounts.

The decreased activity of the catalysts modified with inorganic tin is attributed partly to the blocking of Pd by tin oxide, because the alumina-supported tin monometallic catalyst did not show any activity. However, reaction rates do not correlate well with the amount of CO chemisorption in Table 1. The initial decrease in 1,3-butadiene conversion rate for the catalyst modified by inorganic tin can be understood in terms of deactivation. The catalyst modified by organic tin containing carbon species was deactivated less than the catalyst modified by inorganic tin.

Enhanced 1-butene selectivities, regardless of the nature of the tin precursor, may be due to hydrogen availability. In hydrogenation of acetylene the increase in ethene selectivity on polymer-covered palladium black has been attributed to the decreased surface hydrogen availability as a consequence of the low solubility of hydrogen in the polymer film (28). Noting that the addition of tin reduced the edge energy of palladium and thus suppressed the formation of the β-hydride phase of palladium irrespective of the nature of tin precursor, similar 1-butene selectivities could be attributed to similar hydrogen availability.

Despite similar hydrogen availability, a higher selectivity for *n*-butane for the catalyst modified by inorganic tin compared to that modified by organic tin could be understood by a difference in the Pd–Sn interaction as manifested by the Sn–Pd coordination numbers. The EXAFS fitting showed greater Sn–Pd coordination numbers for catalysts modified with organic tin. The added tin might destroy the Pd ensemble in catalysts which are active for total hydrogenation of 1,3-butadiene. The increased interaction between Sn and Pd represented by a large Sn–Pd coordination number would suppress more effectively total hydrogenation of 1,3-butadiene to *n*-butane.

CONCLUSION

XAFS demonstrated the changes in electronic and geometric structures of alumina-supported palladium catalysts when tin was added. Regardless of the nature of the tin precursor, tin modification suppressed the formation of the palladium β-hydride phase. The added tin destroyed palladium ensembles on alumina by making Pd–Sn bonds. These effects had a positive role in increasing 1-butene selectivity for the hydrogenation of 1,3-butadiene and decreasing the formation of *n*-butane. Carbonaceous species was formed in catalysts modified with organic tin, while the modification using inorganic tin precursors generated oxide-like species in addition to making Sn–Pd bonds. Thus palladium catalysts modified with different tin precursors showed different

activity and selectivity patterns in the hydrogenation of 1,3-butadiene.

ACKNOWLEDGMENTS

We appreciate Dr. M. Nomura's help during XAFS experiments in the Photon Factory.

REFERENCES

1. Meyer, E. F., and Burwell, R. L., *J. Am. Chem. Soc.* **85**, 2881 (1963).
2. Riley, M. G., Ph.D. thesis, Rice University, Houston, TX, 1989.
3. Sárkány, A., Zsoldos, Z., Furlong, B., Hightower, J. W., and Guczi, L., *J. Catal.* **141**, 566 (1993).
4. Sárkány, A., Zsoldos, Z., Stefler, Jy., Hightower, J. W., and Guczi, L., *J. Catal.* **157**, 179 (1995).
5. Furlong, B., Hightower, J. W., Chan, T. Y.-L., Sárkány, A., and Guczi, L., *Appl. Catal. A* **117**, 41 (1994).
6. Meitzner, G., Via, G. H., Lytle, F. W., Fung, S. C., and Sinfelt, J. H., *J. Phys. Chem.* **92**, 2925 (1988).
7. Hobson, M. C., Jr., Goresh, S. L., and Khare, G. P., *J. Catal.* **142**, 641 (1993).
8. Margitfavi, J., Szabó, S., Nagy, F., Göbölös, S., and Hegedüs, M., *in* "Preparation of Catalysts III" (G. Poncelet, P. Grange, and P. A. Jacobos, Eds.), p. 473. Elsevier, Amsterdam, 1983.
9. Margitfavi, J., Kern-Tálas, E., and Göbölös, S., "Proceedings of the XIIth International Conference on Organometallic Chemistry, Vienna, September, 1985," p. 518.
10. Didillon, B., Houtman, C., Shay, T., Candy, J. P., and Basset, J. P., *J. Am. Chem. Soc.* **115**, 9380 (1993).
11. Lesage, P., Clause, O., Moral, P., Didillon, B., Candy, J. P., and Basset, J. P., *J. Catal.* **155**, 238 (1995).
12. "X-ray Absorption: Principles, and Applications and Techniques of EXAFS, SEXAFS and XANES" (D. C. Koningsberger and R. Prins, Eds.), Wiley, New York, 1988.
13. Stytsenko, V. D., *Appl. Catal. A* **126**, 1 (1995).
14. Lee, J. S., Choi, S. H., Kim, K. D., and Nomura, M., *Appl. Catal. B* **7**, 199 (1996).
15. Nomura, M., KEK Report 85-7 (1985).
16. Nomura, M., and Koyama, A., KEK Report 89-16 (1989).
17. Stern, E. A., Newville, M., Ravel, B., Yacoby, Y., and Haskel, D., *Physica B* **208** & **209**, 117 (1995).
18. Rehr, J. J., Mustre de Leon, J., Zabinsky, S. I., and Albers, R. C., *J. Am. Chem. Soc.* **113**, 5135 (1991).
19. "International Tables for X-ray Crystallography" (C. H. MacGillavry, D. Rieck, and K. Lonsdale, Eds.), Vol. III. Reidel, Dordrecht, 1985.
20. "Dictionary of Inorganic Compunds" (J. E. Macintyer, Ed.), Chapman & Hall, New York, 1992.
21. Hyde, B. G., and Anderson, S., "Inorganic Crystal Structure," p. 67. Wiley, New York, 1989.
22. Van den Berg, J. M., *Acta Crystallogr.* **14**, 1002 (1961).
23. Fujii, H., and Kimura, M., *Bull. Chem. Soc. Jpn.* **43**, 1933 (1970).
24. Wicke, E., and Brodowsky, H., *in* "Hydrogen in Metals II" (G. Alefeld and J. Vlkl, Eds.), p. 73. Springer-Verlag, Berlin, 1978.
25. Davis, R. J., Landry, S. M., Horsley, J. A., and Boudart, M., *Phys. Rev. B* **39**, 10580 (1989).
26. Nédez, C., Lefebvre, F., Choplin, A., Niccolai, G. P., Basset, J. M., and Benazzi, E., *J. Am. Chem. Soc.* **116**, 8638 (1994).
27. Humbolt, F., Didillon, D., Lepeltier, F., Candy, J. P., Corker, J., Clause, O., Bayard, F., and Basset, J. M., *J. Am. Chem. Soc.* **120**, 137 (1998).
28. Sárkány, A., Cuczi, L., and Weiss, A. H., *Appl. Catal.* **10**, 369 (1984).